

# Plasma Sprayed High Lubricity Nanocomposite Coatings

X. Q. Ma, T. DeCarmine, T. D. Xiao, Inframat Corporation, Farmington/U.S

A typical high-pressure fuel pump for direct injection (DI) engines operates with fuels such as petroleum-based hydrocarbons that have inherent lubricating properties. However, environmental requirements put the thrush to use cleaner fuels that don't contain lubricants and consequently an increasing abrasion problem presents with the surface of high-pressure fuel pump for direct injection engines. To alleviate this problem, the alternative solution was proposed to promote wear and corrosion resistance of DI engines by applying high-lubricity coatings onto surfaces of engine components such as pump plungers. In this work, self-lubricating nanocomposites with nano- $\text{Al}_2\text{O}_3/\text{TiO}_2$  matrix and  $\text{Fe}_3\text{O}_4$  additive as solid lubricant was the first proposed. The nanocomposites had been fabricated into lubricant coatings with a single layer or a functionally graded structure in plasma spray process. Tribological test results for the nanocomposite coatings demonstrated 4 times increase in sliding wear resistance and 3-5 times increase in abrasive wear resistance in under the tested conditions. The lowest coefficient of friction about 0.18 was measured on the nanocomposite coating with an optimal  $\text{Fe}_3\text{O}_4$  content in pin-on-disk test in ethanol. Based on morphologies and wear behavior analyses, the wear mechanism was proposed for the nanocomposites. The nanocomposite coatings have exhibited the advantages of cleavability, chemical stability, low friction and high wear resistance, and will have a potential for various applications that require high lubricity at ambient and elevated temperature.

## 1 Introduction

High-pressure fuel pumps for direct injection (DI) engines typically operate with fuels, such as petroleum based hydrocarbons, that have inherent lubricating properties. Fuel injection of hydrocarbon-based liquids does not induce a wear problem with the surfaces of fuel pumps. As environmental requirements drive the need to move to cleaner fuels, liquids with non-lubricating properties will be the working fluid in high pressure DI fuel pumps. These clean-burning fuels are ether and alcohol based fuels such as methanol and ethanol. These fuels have no inherent lubricating properties and it would defeat the object of clean burning fuels to add a sacrificial lubricating component to cope with lubrication. An alternative is to develop corrosion and abrasion resistant high-pressure pumps with lubricity incorporated into the contacting and sliding surfaces of the pump.

Solid lubricant coatings in common use include non-oxide type solid lubricants and oxide type solid lubricants, and both are currently used in advanced military aircraft, as well as civilian applications, which include utility power stations, a variety of pumps, diesel engines and gear trains [1-5]. Common non-oxide solid lubricants are referred to layered materials such as graphite,  $\text{MoS}_2$  and  $\text{WS}_2$  [6-8]. Compared to lubricants in liquid or grease forms or non-oxide solid lubricants, oxide type solid lubricant have the advantages of less or no contamination and evaporation, high stability and oxidation resistance at elevated temperature, providing practical and adequate applications for high vacuum apparatus, aerospace, mobile, medical and food devices. Further, those solid lubricants can be dispersed into metal or ceramic matrix to form dual-phase lubricant coatings. Ceramic coatings have the greatest long-term growth potential for improved wear and corrosion resistances in diesel engine components for ships, urban buses, locomotives, earth moving vehicles, and power

generating stations, and thereby have a strong economic thrush and environmental impact. In comparison to conventional ceramic coatings, nanostructured ceramic coatings like  $n\text{-Al}_2\text{O}_3/\text{TiO}_2$  have demonstrated superior performance in terms of wear, erosion and corrosion as well as mechanical properties [9-12]. In this work, oxide additive acting as "soft" lubricant phase was introduced to nanostructured alumina/titania matrix for forming a self-lubricant nanocomposite coating. The major aim was to reduce friction while keeping wear resistance high. Eventually, the single layered and functionally gradient nanocomposite coatings were fabricated by plasma spray technology, and their friction and wear behaviors were evaluated.

## 2 Experimental Procedures

### 2.1 Materials

Substrate material used was carbon steel 1030, which was cut into rectangular coupons with the dimensions of  $50 \times 75 \times 1 \text{ mm}^3$ . Nanostructured  $\text{Al}_2\text{O}_3/13\text{wt.}\% \text{TiO}_2$  was synthesized by Inframat Corporation (Connecticut, U.S) and micrometer sized  $\text{Fe}_3\text{O}_4$  was purchased from Alfa Aesar (Massachusetts, U.S). These powders were blended, ball-milled and reconstituted into feedstock in spray dry process. Nano- $\text{Al}_2\text{O}_3/13\text{TiO}_2$  and  $\text{Fe}_3\text{O}_4$  feedstock also were prepared in the same procedure. For the composite agglomerates, the content of  $\text{Fe}_3\text{O}_4$  component was 15, 25, 50 and 75% in weight, respectively. Prior to plasma spraying, the substrates were sand blasted with aluminum oxide grits and then ultrasonically cleaned with acetone.

### 2.2 Plasma spray

Plasma spraying of nanostructured  $\text{Al}_2\text{O}_3/\text{TiO}_2$ ,  $\text{Fe}_3\text{O}_4$  and  $n\text{-Al}_2\text{O}_3/\text{TiO}_2 + \text{Fe}_3\text{O}_4$  composite agglomerates was carried out with a 9MB plasma gun (Sulzer-Metco, NY,

U.S). Plasma spray parameters were optimized with Ar/H<sub>2</sub> working gases. The major spray parameters for these powders are given in Table 1. The single-layered coatings were deposited up to 250-300µm, and the graded coating of *n*-Al<sub>2</sub>O<sub>3</sub>/TiO<sub>2</sub>+Fe<sub>3</sub>O<sub>4</sub> was deposited up to 900µm with increasing Fe<sub>3</sub>O<sub>4</sub> content from the bottom 15%, the middle 35% to the top 50%.

**Table 1.** Plasma spray parameters for applying these ceramic coatings

Parameters	Feedstock Materials		
	<i>n</i> -Al <sub>2</sub> O <sub>3</sub> /TiO <sub>2</sub>	Fe <sub>3</sub> O <sub>4</sub>	Composite
Ar Flow SCFH	100	120	80
H <sub>2</sub> Flow SCFH	26	21	33
Voltage, V	550	500	600
Current, A	70	70	70
Standoff mm	90	100	90
Feedrate Kg/h	2.3	2.3	1.8

### 2.3 Friction test

Friction coefficients  $\mu$  of the sprayed coatings were measured in pin-on-disk tests according to ASTM standard G99-95A. A tribometer (LSC-200PC, Implant Sciences Corp., Massachusetts, U.S) was employed to measure the coefficients  $\mu$  with a setup of the coated disk sample (32mm in diameter) against a carbon steel ball (1030, 16mm in diameter). The test conditions included test loading 250grams, disk rotation 80rpm and wear track diameter 15mm. The friction test was conducted by immersing whole test coupon and mating pin in ethanol. The total revolution number was up to 10,000. Prior to the friction tests, the coating samples were grinded and finally polished using 2µm alumina paste.

### 2.4 Abrasive wear test

A diamond abrasive pad (grain size 40µm, 170mm in diameter) was used as abrasive disk and a stream of ethanol was injected onto the pad via a liquid dozer. The coated disk samples with a diameter of 32mm were fixed in a specimen mover which rotated counter-clock relatively to the abrasive pad. When the test was started, the tested samples were loaded at 90N. The weight changes of the tested samples were measured with a high precision balance and were used to quantize wear losses of the samples.

### 2.5 Coating characterization

The surfaces and the cross-sections of the coatings tested and not were observed by scanning electronic microscopy (SEM). The worn surfaces were observed by SEM as well. The depth and width of wear tracks on the worn surfaces were measured by a profilometer. X-ray diffraction (XRD) analysis was used to identify phase compositions in the coatings.

## 3 Results and Analyses

### 3.1 Microstructures

The representative SEM micrographs of as-sprayed coatings are exhibited in Fig.1. *n*-Al<sub>2</sub>O<sub>3</sub>/TiO<sub>2</sub> coating usually is crack-free and adheres well to the substrate and there is no visible inclusion of unmelt particles. The coating porosity was estimated as 5%. The presence of open porosity was mostly attributed to the partially melting of feedstock particles and not fully deforming into pancake-like splats as observed using SEM tomography. XRD analysis indicated that the ceramic coating consisted of  $\alpha$  and  $\gamma$  phases, and there was no peak identified for TiO<sub>2</sub>. As revealed in previous studies [13], the absence of TiO<sub>2</sub> phase (r-rutile or t-anatase) was caused by the negligible solubility of TiO<sub>2</sub> in the equilibrium  $\alpha$ -alumina and possible existence of Ti ions in the  $\gamma$ -alumina lattice as either an interstitial or substitutional defects. In Fig. 1a, a dense Fe<sub>3</sub>O<sub>4</sub> coating is exhibited with porosity less than 1%. The improvement in coating density should come from a fully melting of Fe<sub>3</sub>O<sub>4</sub> feedstock most likely due to its low melting point 1594°C. In addition, the sprayed Fe<sub>3</sub>O<sub>4</sub> coating had a much smooth surface, indicating good flattening and well wetting of the melted droplets during coating built-up.

In the nanocomposite coatings shown in Fig. 1b and 1c, the overlapped lamellas of two distinct phases can be easily identified. The dark phase is Al<sub>2</sub>O<sub>3</sub>/TiO<sub>2</sub> and the grey is Fe<sub>3</sub>O<sub>4</sub>. Some outstanding microstructural features were identified for the composite coatings: (1) Full density. With increasing Fe<sub>3</sub>O<sub>4</sub> content (>50%), the composite coating was fully dense with few porosity. This improvement should be attributed to the fully melting and well flattening of Fe<sub>3</sub>O<sub>4</sub> as a secondary phase in *n*-Al<sub>2</sub>O<sub>3</sub>/TiO<sub>2</sub> matrix; (2) Good coating integrity. The coatings had few microcracks and exhibited good cohesion at *n*-Al<sub>2</sub>O<sub>3</sub>/TiO<sub>2</sub> and Fe<sub>3</sub>O<sub>4</sub> interpass boundaries. It was verified that the Fe<sub>3</sub>O<sub>4</sub> phase was much softer (HV<sub>300</sub>=510) than *n*-Al<sub>2</sub>O<sub>3</sub>/TiO<sub>2</sub> phase (HV<sub>300</sub>=920) and thus the spray nanocomposites had a high strain tolerance to thermal or quenching stress induced during spraying and solidifying, and (3) perfect interfacial bonding at the coating and substrate interface. Moreover, the retaining of original Fe<sub>3</sub>O<sub>4</sub> phase structure was verified in the plasma sprayed Fe<sub>3</sub>O<sub>4</sub> coating by XRD analysis. In term of material characteristics, *n*-Al<sub>2</sub>O<sub>3</sub>/TiO<sub>2</sub> and Fe<sub>3</sub>O<sub>4</sub> will provide wear resistance and lubricity, respectively. A functionally gradient nanocoating was proposed to provide compliance in coating structure and coating function while the surface requires high lubricity and low wear rate. The graded *n*-Al<sub>2</sub>O<sub>3</sub>/TiO<sub>2</sub>

+Fe<sub>3</sub>O<sub>4</sub> coating was prepared by multi-layer deposition of *n*-Al<sub>2</sub>O<sub>3</sub>/TiO<sub>2</sub> with 0, 15, 35 and 50wt.% Fe<sub>3</sub>O<sub>4</sub> in sequence.

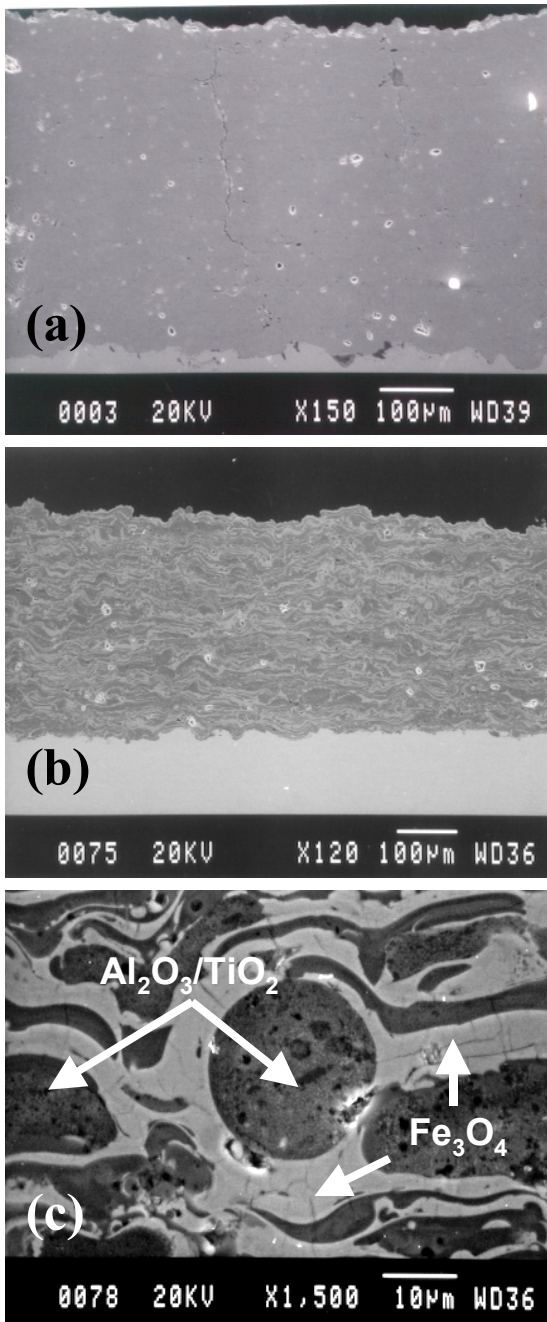


**Fig. 1:** SEM micrographs of as-sprayed solid lubricant coatings. (a) Fe<sub>3</sub>O<sub>4</sub> coating; (b) *n*-Al<sub>2</sub>O<sub>3</sub>/TiO<sub>2</sub>+50%Fe<sub>3</sub>O<sub>4</sub> nanocomposite; (c) *n*-Al<sub>2</sub>O<sub>3</sub>/TiO<sub>2</sub>+50%Fe<sub>3</sub>O<sub>4</sub> nanocomposite, x1,500

Each layer was deposited up to 150-200 μm, and the total thickness up to 900μm. The gradient microstructure of the nanocomposite coating is demonstrated in Fig. 2. In the SEM micrograph, the increase in Fe<sub>3</sub>O<sub>4</sub> content from the bottom to the top is clearly indicated. The interfaces between the multiple layers can not be told from interfacial markers such as crack and pore defects and so indicates an ideal

connection situation in the graded coating. Another outstanding feature is that there is no visible vertically crack in the graded coatings. This observation implies that there is a low level of residual stress in the coating and it will be a favorite factor in consideration of its improved friction and wear resistance as well as microstructural integrity and reliability.

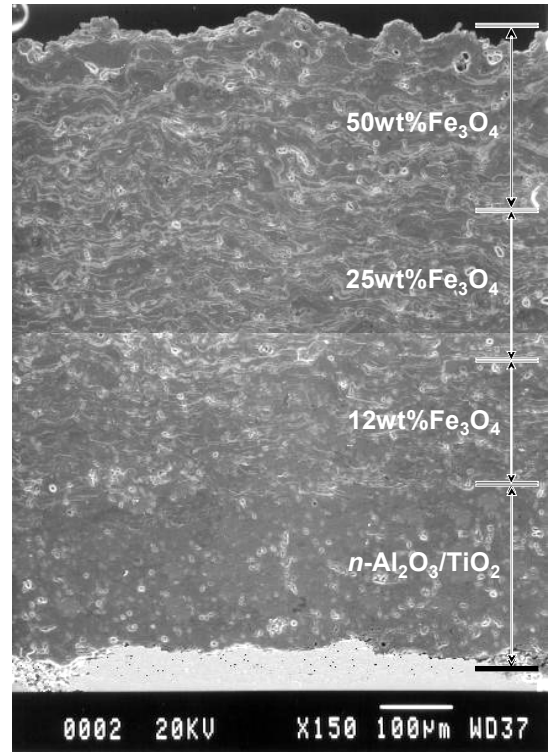


**Fig. 2:** Functionally gradient nanocoating of *n*-Al<sub>2</sub>O<sub>3</sub>/TiO<sub>2</sub> with Fe<sub>3</sub>O<sub>4</sub> solid lubricant fabricated by air plasma spray

### 3.2 Friction behaviors

Friction coefficients of the sprayed coatings were measured in pin-on-disk tests at room temperature in ethanol, and the typical plots of friction coefficient versus revolution for various coatings are presented in Fig.3. For carbon steel 1030, a constant friction coefficient was measured within 1000 revolutions, however, there was a dramatic fluctuation in the coefficient after 2000 revolutions. The highest coefficient 0.29 was measured after 5000s, in parallel with the presence of surface rusting and deeply worn track. The results should be attributed to the formation of brittle rust and the great change in contact area between the steel disk and the ball pin which both suffered a several adhesive wear and produced some debris-induced plunges. The phenomenon of dynamic change in coefficient values reflects the increase or reduction in friction force corresponding to the debris formation and removal from the worn track respectively. This result confirms that carbon steel will definitely experience several wear damage if its surface is not protected by suitable coating in the medium of alcohol fuel.

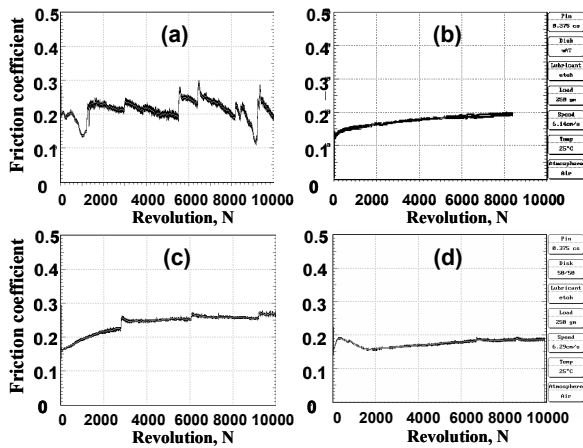


**Fig. 3:** The coefficients of carbon steel and the plasma sprayed lubricant coatings tested in pin-on-disk in ethanol. (a) Carbon steel 1030; (b)  $n\text{-Al}_2\text{O}_3/\text{TiO}_2$  nanocoating; (c)  $\text{Fe}_3\text{O}_4$  coating; (d) nanocomposite coating with 50wt%  $\text{Fe}_3\text{O}_4$

The initial coefficient  $\mu$  of the  $\text{Fe}_3\text{O}_4$  coating was about 0.16, then increased steadily with revolution and eventually was constant about 0.27. There was a step increase in the  $\mu$  value every 3,000 revolutions. For the exploitation of the phenomena, it is worthy to mention that the coefficient of the  $\text{Fe}_3\text{O}_4$  coating was quite lower ( $\mu=0.1$ ) in dry condition than in ethanol. In the case of friction test in ethanol, somewhat wet "slurry" was induced and accumulated around the worn tracks with increasing time. It is assumed that the slurry was introduced from the fine debris of worn  $\text{Fe}_3\text{O}_4$  particles, and thereafter friction force increased due to an adhesive attachment of the slurry debris to both the pin ball and the tested coating. The periodic fluctuation in  $\mu$  actually reflects the repeated procedure of adhesion and detachment of the wet debris. Based on the result of the friction experiment, it is proved that a simple  $\text{Fe}_3\text{O}_4$  coating is not a suitable candidate for high-lubricity material in DI engines using alcohol fuels.

$n\text{-Al}_2\text{O}_3/\text{TiO}_2$  coating and its composite coatings with  $\text{Fe}_3\text{O}_4$  additive had the similar low friction coefficient among the tested coatings,  $\mu$  value ranging from initial 0.12-0.15 to 0.18-0.2 at 10,000 revolutions. The effect of  $\text{Fe}_3\text{O}_4$  content on the coefficient of friction and microhardness had been investigated. In Fig. 4, the coefficients of friction of the composite coatings tend to decrease with increasing  $\text{Fe}_3\text{O}_4$  content. When  $\text{Fe}_3\text{O}_4$  content exceeds 50%, the coefficients are nearly constant. There is no simple relation between coefficient of friction and microhardness for the nanocomposite coatings.

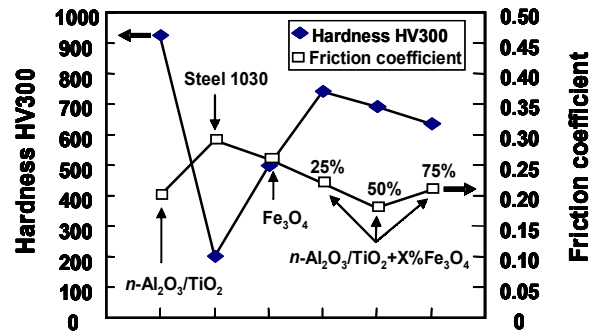


**Fig.4:** Correlation between coefficients of friction and microhardness of the tested coating samples in pin-on-disk

### 3.3 Observation of worn surfaces

The worn tracks on those plasma sprayed coatings had been characterized according to their morphologies and profilometries. The SEM morphologies of the worn surfaces after pin-on-disk testing are selectively shown in Fig.5. The worn

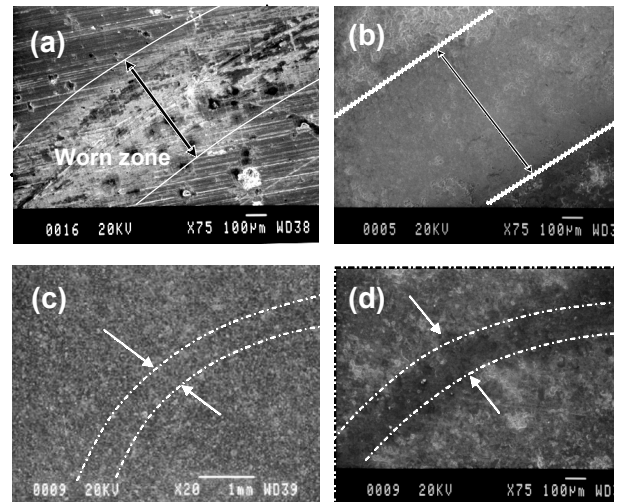


**Fig.5:** SEM observation of worn surfaces of the material and coatings after tested in pin-on-disk tests. (a) Carbon steel 1030; (b)  $\text{Fe}_3\text{O}_4$  coating; (c)  $n\text{-Al}_2\text{O}_3/\text{TiO}_2$  nanocoating (d) Nanocomposite coating with addition of 75wt%  $\text{Fe}_3\text{O}_4$

tracks on carbon steel and  $\text{Fe}_3\text{O}_4$  coating are much wider (3-5 times) than those on  $n\text{-Al}_2\text{O}_3/\text{TiO}_2$ -based coatings. The worn track on  $n\text{-Al}_2\text{O}_3/\text{TiO}_2$  is indistinct, in contrast, that on composite coating is nearly invisible while keeping the track narrow. The morphologies indicated that the surface on carbon steel was severely worn and deformed with the evidence of plastic deformation and material removal. The surface of  $n\text{-Al}_2\text{O}_3/\text{TiO}_2$  coating was smooth without distinct damages like scratches, grooves, deformation, delamination and brittle fracture, which was consistent with the previous observation [10]. In contrast, the friction track on  $\text{Fe}_3\text{O}_4$  coating was entirely smooth with evidence of plastic deformation

referring to very fine scratching, locally pull-out of tiny debris and plastic smearing, but with exemption of microcracking and delamination. The nanocomposite coating had exhibited the combined morphological features of  $n\text{-Al}_2\text{O}_3/\text{TiO}_2$  and  $\text{Fe}_3\text{O}_4$  coatings. On the composite coating containing 75% $\text{Fe}_3\text{O}_4$ , the smearing film of  $\text{Fe}_3\text{O}_4$  covered entirely friction track and there was no  $n\text{-Al}_2\text{O}_3/\text{TiO}_2$  exposed locally, which was similar to the situation on  $\text{Fe}_3\text{O}_4$  coating.

### 3.4 Wear rates in pin-on-disk tests

Pin-on-disk tests were carried out under normal load 2.45N at a constant sliding speed of 65 mm/s in ethanol. After 10,000 revolutions, the geometric profiles of the worn tracks were measured by a profilometer. The wear rates were calculated from the weight losses of the tested samples and the profiles of the friction tracks. Figure 6 presents the plots of wear rates of carbon steel and the coating samples. Carbon steel has the highest wear rate about  $1.3 \times 10^{-7} \text{ mm}^3/\text{N}\cdot\text{mm}$ . The wear rate of  $\text{Fe}_3\text{O}_4$  coating is about  $0.41 \times 10^{-7} \text{ mm}^3/\text{N}\cdot\text{mm}$ , i.e. 3 times lower than that of carbon steel. With the addition of  $\text{Fe}_3\text{O}_4$  to  $n\text{-Al}_2\text{O}_3/\text{TiO}_2$  matrix, a dramatic reduction in the wear rate occurred in all the composite coatings. The wear rate continued to decrease with increasing  $\text{Fe}_3\text{O}_4$  content and reached the lowest in the coating with 50% $\text{Fe}_3\text{O}_4$ . With a further increase of the  $\text{Fe}_3\text{O}_4$  amount to 75%, the wear rate rose inversely to  $0.38 \times 10^{-7} \text{ mm}^3/\text{N}\cdot\text{mm}$  that was comparable to that of  $\text{Fe}_3\text{O}_4$  coating. In terms of friction coefficient and wear rate, the optimal composition for the composite coating was determined as  $n\text{-Al}_2\text{O}_3/\text{TiO}_2+50\%\text{Fe}_3\text{O}_4$ .

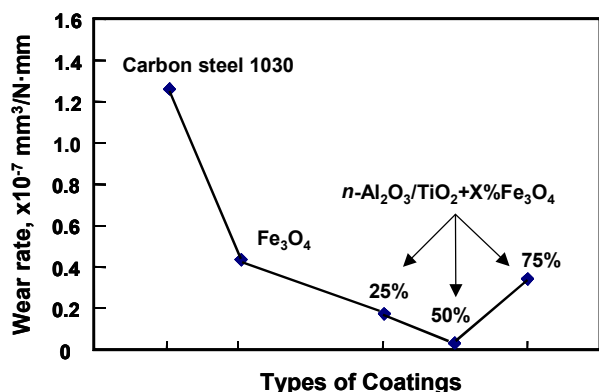


Fig. 6: Comparison on the wear rates of various sprayed coatings tested in pin-on-disk in ethanol

### 3.5 Abrasive wear property

Abrasive tests were conducted by using a  $40 \mu\text{m}$  diamond abrasive pad against the coating samples. Meanwhile, a stream of ethanol was injected onto the pad via a liquid doser. In Fig. 7, the plots of weight loss versus time are compared among  $n\text{-Al}_2\text{O}_3/\text{TiO}_2$  coatings with different  $\text{Fe}_3\text{O}_4$  contents. In general, the wear rates increase linearly with testing time for all the

samples. While carbon steel 1030 had shown the highest weight loss within the testing period, the composite coatings had less weight losses for all the contents, especially for the nanocomposite with 50%  $\text{Fe}_3\text{O}_4$  content that had the lowest weight loss even compared to  $n\text{-Al}_2\text{O}_3/\text{TiO}_2$ . With the increase in testing time, the difference in weight loss among the samples became remarkable. The weight loss was not proportional to the  $\text{Fe}_3\text{O}_4$  content; the coatings containing 25% and 75%  $\text{Fe}_3\text{O}_4$  had demonstrated a relatively higher weight loss than the coating having an intermediate content of 50%  $\text{Fe}_3\text{O}_4$ . There was no a consistence between the wear rates in pin-on-disk tests and the abrasive wear data for most of the tested samples.

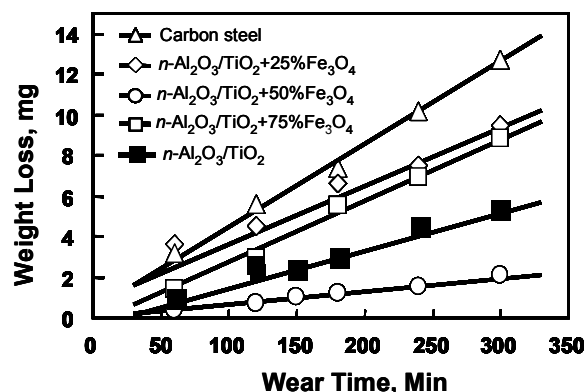


Fig. 7: Plots of weight loss vs wear time for the plasma sprayed coatings tested against abrasive diamond-contained mate in ethanol

### 3.6 Friction mechanism

Some literatures were related to the use of iron particles and iron oxides as lubricant media for high-temperature applications [14-19], however, it is the first time to report the manufacture and the friction and wear behavior of nanostructured  $\text{Al}_2\text{O}_3/\text{TiO}_2$  matrix with  $\text{Fe}_3\text{O}_4$  additive as solid lubricant. The effects of iron particles on the friction and wear mechanisms of ceramics in ethanol was reported by T. Hisakado [20], and it was found that the addition of iron particles in ethanol decrease the wear rates of SiC and TiC disks and pins. Ouyang et al. reported the microstructure and tribological properties of low-pressure plasma-sprayed  $\text{ZrO}_2$  with  $\text{CaF}_2$  and  $\text{Ag}_2\text{O}$  lubricants at elevated temperatures, and revealed that  $\text{Ag}_2\text{O}$  and  $\text{CaF}_2$  acting as solid lubricants were effective at  $300\text{-}700^\circ\text{C}$ , and brittle fracture and delamination were demonstrated to be the dominant wear mechanism at room temperature [21].

At room temperature, microfracture-controlled wear process is dominant wear mechanism for most ceramic coatings due to their inherent high brittleness and low strain tolerance. In our studies,  $n\text{-Al}_2\text{O}_3/\text{TiO}_2$  plasma sprayed coating was verified to have a high toughness, cohesive and adhesive bonding strength. As a result, the improved brittleness and integrity of the nanostructured coating was responsible for

improved friction and wear properties due to nanoscale plastic deformation, reduced microfracture, delamination and grain tearing-out. It is generally accepted that the wear behavior of a materials is directly related to its microhardness, toughness, grain size, mating material properties and especially microstructure and defects (porosity, unmelt particles and lamellar splat boundary) for thermal sprayed coatings. From the results presented in Fig.4, 6 and 7, it was concluded that the coefficients of friction and wear rates of the nanocomposite coatings were not simple related to their microhardness.  $n\text{-Al}_2\text{O}_3/\text{TiO}_2+50\%\text{Fe}_3\text{O}_4$  with a moderate microhardness ( $\text{HV}_{300}=700$ ) had demonstrated the lowest coefficient  $\mu$  and wear rate, however, the improvement should not be much related to the coating porosity and defects because the coatings were deposited with a well melted and nearly full dense microstructure in the tested conditions.

To further elucidate the wear mechanism, the close observation on the friction tracks of  $n\text{-Al}_2\text{O}_3/\text{TiO}_2$  coating and its nanocomposite with  $50\%\text{Fe}_3\text{O}_4$  are compared in Fig. 8. The worn surface on  $n\text{-Al}_2\text{O}_3/\text{TiO}_2$  was smooth with few grooving and grain pull-off,

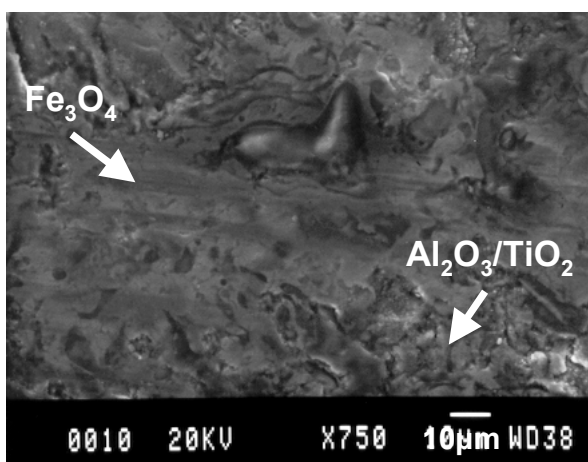
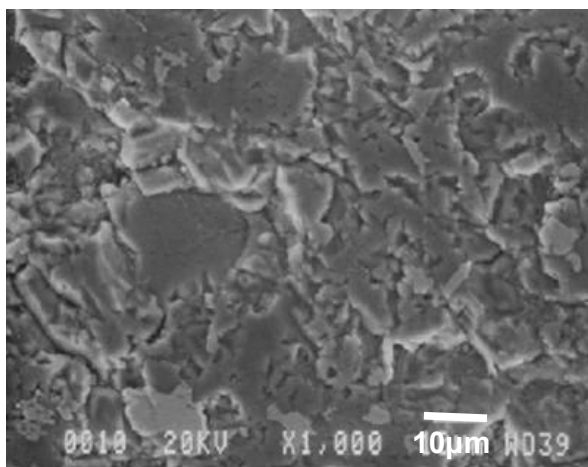


**Fig. 8:** SEM morphologies of the worn surfaces on (a)  $n\text{-Al}_2\text{O}_3/\text{TiO}_2$  nanocoating and (b) nanocomposite coating with  $75\%\text{Fe}_3\text{O}_4$  after pin-on-disk testing for 10,000 revolutions.

and so implied that the wear damages due to

microfracture and associated splat/grain detachment were inhibited to a great extent. With the addition of  $\text{Fe}_3\text{O}_4$  to  $n\text{-Al}_2\text{O}_3/\text{TiO}_2$  matrix, a transferred  $\text{Fe}_3\text{O}_4$  film was formed and thereafter covered the wear surface partially (the case of 25 and 50%  $\text{Fe}_3\text{O}_4$  addition) and completely (the case of  $75\%\text{Fe}_3\text{O}_4$  addition) as schematically shown in Fig. 9. From the viewpoint of microstructure and coating integrity, the presence of “soft”  $\text{Fe}_3\text{O}_4$  phase should promote perfect

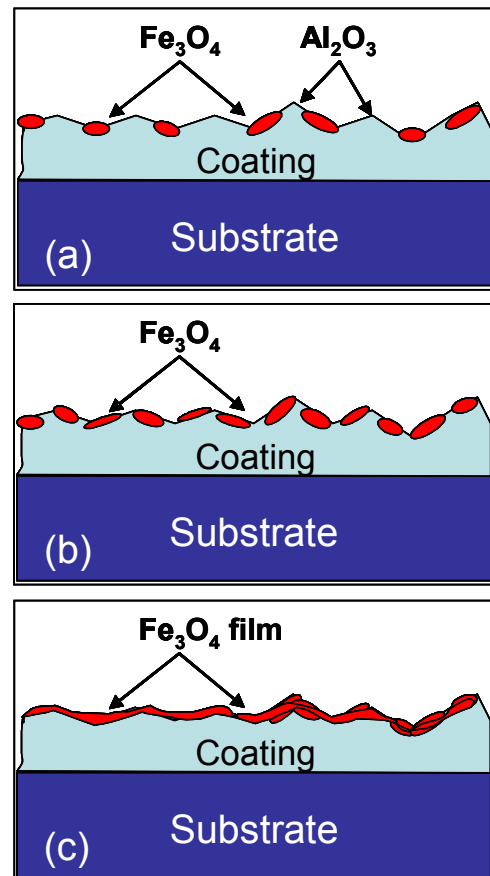


**Fig. 9:** Schematic of “hard” and “soft” regions on the worn surfaces of nanocomposite coatings. (a) isolated two regions in the case of a low  $\text{Fe}_3\text{O}_4$  content; (b) Predominant surface covered by  $\text{Fe}_3\text{O}_4$  in the case of moderate  $\text{Fe}_3\text{O}_4$  content; (c) Completed surface covered by “soft”  $\text{Fe}_3\text{O}_4$  additive and its transferred film in the case of a high  $\text{Fe}_3\text{O}_4$  content

microstructure by improving melting, wetting and welding between the interpass splats of  $\text{Al}_2\text{O}_3/\text{TiO}_2$  and  $\text{Fe}_3\text{O}_4$  and so resulted in the improvement in coating toughness, strain tolerance and cohesion strength. With a low  $\text{Fe}_3\text{O}_4$  content less than 50%, the worn surface consisted mostly of “hard”  $\text{Al}_2\text{O}_3/\text{TiO}_2$  and an adhesive and/or abrasive wear occurred between the ceramic and the mating carbon steel pin. In the case of a low surface coverage by the  $\text{Fe}_3\text{O}_4$  phase and its transferred film, “hard”  $\text{Al}_2\text{O}_3/\text{TiO}_2$  particles were the majority of wear contact area and dominated the surface wear characteristics, and thus demonstrated the similar friction/wear behaviors to pure  $\text{Al}_2\text{O}_3/\text{TiO}_2$ . With the optimal  $\text{Fe}_3\text{O}_4$  content

namely 50%, part of the wear surface was occupied by  $\text{Fe}_3\text{O}_4$  additive and also smoothed by smeared filling of transferred  $\text{Fe}_3\text{O}_4$ . The combined surface of the "hard" ceramic and major "soft" oxide was confirmed to be beneficial for improving friction and wear properties. When further increasing  $\text{Fe}_3\text{O}_4$  content, the whole surface was covered by  $\text{Fe}_3\text{O}_4$  and the situation became similar to pure  $\text{Fe}_3\text{O}_4$  coating. In the medium of ethanol, the  $\text{Fe}_3\text{O}_4$  debris in slurry form was adhesive to the worn surface and caused an increase in friction force and wear rate. Therefore, the single  $\text{Fe}_3\text{O}_4$  and the composite coating with a high  $\text{Fe}_3\text{O}_4$  content was found not effectively as solid lubricant in ethanol at room temperature under the tested conditions. The potential for the nanocomposite coating as high temperature lubricant will be investigated in the future.

#### 4 Conclusions

1. A self-lubricant nanocomposite coatings with a solid oxide lubricant were developed. The nanocomposite consisted of nano- $\text{Al}_2\text{O}_3/13\text{TiO}_2$  hard matrix and soft  $\text{Fe}_3\text{O}_4$  as lubricant additive. The solid lubricant nanocomposite was designed to provide a low coefficient of friction and high wear resistance as well in the medium of ethanol, and consequently to offer environmental and economic benefits for certain applications like direct injection engines
2. The nanocomposites were fabricated into self-lubricating coatings on carbon steel using plasma spray technology. The nanocomposite coatings were investigated while changing  $\text{Fe}_3\text{O}_4$  contents from 25 to 75wt%. Further, a functionally graded nanocoating was deposited with an optimal concentration of  $\text{Fe}_3\text{O}_4$  on the coating top. The use of  $\text{Fe}_3\text{O}_4$  acting as lubricant additive had resulted in the improvements in microstructure and friction/wear characteristics.
3. Pin-on-disk tests indicated that the friction characteristics of the nanocomposites were distinctly different from those of  $n\text{-Al}_2\text{O}_3/\text{TiO}_2$  and  $\text{Fe}_3\text{O}_4$  coatings. At room temperature, the friction coefficients of the nanocomposite coatings decreased with increasing  $\text{Fe}_3\text{O}_4$  contents from 25% to 50%, but increased inversely with further increasing  $\text{Fe}_3\text{O}_4$  content up to 75%. The wet friction coefficients of the nanocomposites ranged from 0.18 to 0.22, comparable to  $n\text{-Al}_2\text{O}_3/\text{TiO}_2$  coating but much lower than  $\text{Fe}_3\text{O}_4$  coating and carbon steel.
4. Abrasive wear tests demonstrated that the wear resistance of the nanocomposite coatings was superior to  $\text{Fe}_3\text{O}_4$  and even  $n\text{-Al}_2\text{O}_3/\text{TiO}_2$  coatings. The friction and wear properties were related greatly to material chemistry, coating microstructure and mechanical property rather than coating microhardness under the test conditions.
5. SEM morphologies indicated that the surfaces of the worn tracks on the optimal nanocomposites consisted of two distinct regions, i.e. a smooth "soft" region with grooving and smearing of  $\text{Fe}_3\text{O}_4$  and a "hard" region of  $n\text{-Al}_2\text{O}_3/\text{TiO}_2$  without scratching. When there was no  $\text{Fe}_3\text{O}_4$  addition or  $\text{Fe}_3\text{O}_4$  content exceeded 50%, the friction/wear became severely

while the wear contact area was consisted of fully covered by "soft"  $\text{Fe}_3\text{O}_4$  and its transferred film or only "hard"  $\text{Al}_2\text{O}_3/\text{TiO}_2$  splats, respectively.

#### 5 Acknowledgements

The authors gratefully acknowledge financial support by the U.S Environmental Protection Agency under contract No. 68-D-01-025

#### 6 References

- [1] L. Rapoport, Y. Bilik, Y. Feldman, M. Homyonfer, S. R. Cohen and R. Tenne: Hollow nanoparticles of WS as potential solid-state lubricants, *Nature* 87 (1997), pp. 791/793.
- [2] G. D. Gamulya, I. L. Lebedeva, Y. V. Vvedensky and T. P. Yukhno: Secondary structure formation and wear mechanisms for solid lubricant coatings under friction in vacuum, *Wear* 171 (1994), pp. 143/148.
- [3] M. Buchmann, R. Gadow and A. Killinger: Solid lubricant containing coatings for cylinder liners in pressure casted aluminum crankcases in Thermal Spray: Surface Engineering Via Applied Research, Proceedings of the International Thermal Spray Conference, 1st, Montreal, QC, Canada, May 8-11, (2000), pp. 303/308.
- [4] D. Niebuhr, M. Scholl and P. Clayton: Self-lubricating composite plasma sprayed coatings in Thermal Spray: Practical Solutions for Engineering Problems, Proceedings of the National Thermal Spray Conference, 9th, Cincinnati, Oct. 7-11, (1996), pp. 355/361.
- [5] C. Dellacorte: The evaluation of a modified chrome oxide based high temperature solid lubricant coating for foil gas bearings, *Tribology Trans.* 43 (2000), pp. 257/262.
- [6] L. Rapoport, V. Leshchinsky, M. Lvovsky, I. Lapsker, Y. Volovik, Y. Feldman, R. Popovitz-Biro, R. Tenne: Superior tribological properties of powder materials with solid lubricant nanoparticles, *Wear* 255 (2003), pp. 794/800
- [7] D. G. Teer, J. Hampshire, V. Fox, V. Bellido: The tribological properties of  $\text{MoS}_2$ /metal composite coatings deposited by closed field magnetron sputtering, *Surf. Coat. Technol.* 94/95 (1997), pp. 572/577.
- [8] D. Camino, A. H. S. Jones, D. Mercks, D. G. Teer: High performance sputtered carbon coatings for wear resistant applications, *Vacuum* 52 (1999), pp. 125/131.
- [9] B.H. Kear and P. R. Strutt: Nanostructures: The next generation of high performance bulk materials and coatings, *Naval Research Reviews*, XLVI (1994), pp. 4/13
- [10] Y. Wang, S. Jiang, M.D. Wang, T. D. Xiao and P. R. Strutt: Abrasive wear characteristics of plasma sprayed nanostructured alumina/titania coatings, *Wear* 237 (2000), pp. 176/185
- [11] P. Bansal, Nitin P. Padture and A. Vasiliev: Improved interfacial mechanical properties of  $\text{Al}_2\text{O}_3$ -13wt% $\text{TiO}_2$  plasma-sprayed coatings derived from

- nanocrystalline powders, *Acta Mater.* 51 (2003), pp. 2959/2970
- [12] H. Luo, D. Goberman, L. Shaw and M. Gell: Indentation fracture behavior of plasma-sprayed nanostructured  $\text{Al}_2\text{O}_3$ -13wt.% $\text{TiO}_2$  coatings, *Mater. Sci. Eng. A* 346 (2003), pp. 237/245.
- [13] E. H. Jordan, M. Gell, Y. H. Sohn, D. Goberman, L. Shaw, S. Jiang, M. Wang, T. D. Xiao, Y. Wang and P. Strutt: Fabrication and evaluation of plasma sprayed nanostructured alumina-titania coatings with superior properties, *Mater. Sci. Eng. A* 301 (2001), pp. 80/90.
- [14] R.L. Johnson, M. A. Swikert, D.H. Buckley: High-temperature lubrication in reactive atmosphere, *Corrosion* 16 (1960), pp. 395-398.
- [15] H. E. Sliney: Lubricating properties of lead-monoxide-base coatings of various compositions at temperatures to 1250<sup>o</sup>F, NASA Memo 3-2-59E (1959).
- [16] T. Hata: Thin low-friction coatings on iron alloys for service at high temperature, US Patent No. 3514319 (1970).
- [17] K. Omosako, T. Yamada, T. Hiramatsu: Lubricants for hot rolling of stainless steel and preventing the plugging of spray nozzles, Japanese Patent. No. 08199184 (1995).
- [18] H. Kita, T. Murao: Composite ceramics containing dispersed solid lubricants and their manufacture, Japanese Patent No. 10231174 (1997).
- [19] G. Barbezat: Plasma coating running surfaces of combustion engine cylinders for enhanced lubrication, European Patent No. 1340834 (2003).
- [20] T. Hisakado, K. Simizu and H. Suda: The effects of iron particles on the friction and wear mechanisms of ceramics in ethanol, *Wear* 210 (1997), pp. 188/194.
- [21] J. H. Ouyang, S. Sasaki and K. Umeda: Microstructure and tribological properties of low-pressure plasma-sprayed  $\text{ZrO}_2$ - $\text{CaF}_2$ - $\text{Ag}_2\text{O}$  composite coating at elevated temperature, *Wear* 249 (2001), pp. 440/451.